ISSN 0027-1349, Moscow University Physics Bulletin, 2024, Vol. 79, Suppl. 2, pp. S630–S638. © Allerton Press, Inc., 2024.

Encoding of Input Signals in Terms of Path Complexes in Spiking Neural Networks

V. A. Ilyin[1,2,3*], Ya. P. Ivina[1], M. Yu. Khristichenko[1], A. V. Serenko[1], and R. B. Rybka[1]

[1] *National Research Centre "Kurchatov Institute," Moscow, 123182 Russia*
[2] *National Center for Cognitive Research, ITMO University, St. Petersburg, 197101 Russia*
[3] *Research Computing Center, Lomonosov Moscow State University, Moscow, 119991 Russia*

Received October 1, 2024; revised October 10, 2024; accepted October 20, 2024

Abstract—The article proposes a method for encoding input signals in a spiking neural network based on the mathematics of path complexes on directed graphs. The hypothesis formulated is that when the input signal is repeatedly applied, the STDP dynamics increases synaptic weights along the pathways of active neurons, while the weights of other synaptic connections decrease. As a result, a directed subgraph (path complex) is appearing for each input signal consisting of edges with large synaptic weights. Such path complexes should be unique for different input signals. This hypothesis is confirmed by the example of a simple spiking neural network model, for which a relevant parameter window has been found. Two methods of comparing path complexes (input signals encodings) are proposed. The first one is based on the introduction of the Euclidean metric on a set of path complexes, and the computation of distances between path complexes. The second one consists of compiling the algebra-topological portraits of path complexes—simplexes and homologies, and their subsequent comparison. The proposed method of encoding input signals is, in fact, a new tool that can be considered as an initial stage in the development of a new type of approaches to data analysis.

Keywords: spiking neural network, STDP, signal encoding, digraph, path complex, Euclidean metric, simplex, homology

DOI: 10.3103/S0027134924702084

1. INTRODUCTION

Spiking neural networks are a separate class of artificial neural networks in which neurons interact through the transmission of short-term impulses (spikes) [1] through synaptic connections, thereby simulating neuronal processes in the brain.

As a mathematical structure, spiking neural networks are directed graphs (digraphs) [2]. A dynamic system is implemented on digraphs, in which there are two types of interacting elements—neurons (digraph vertices) and synaptic connections between neurons (directed edges of the digraph). The spiking neural network is a dynamic system, unlike other types of artificial neural networks in which there are no internal processes developing over time.

The synaptic connection is characterized by the time of transmission of the spike along the corresponding edge of the digraph t_{syn} (synaptic delay). The dynamic state of the synaptic connection is set by such a parameter as ω (synaptic weight). Its value affects the change in the dynamic state of the neuron at the moment when a spike arrives at it through this synaptic connection. In our studies, the values of synaptic weights are limited by the interval $0 < \omega < 1$.

The dynamic state of a neuron changes at the moment when the spike arrives along the incoming edge and at the moment when this neuron emits a spike, which is transmitted along the outgoing synaptic connection. In this article the Leaky Integrate-and Fire neuron model [3] is used, in which the neuron dynamics is set by the membrane potential, limited by the upper threshold value. Upon arrival of an incoming spike, the membrane potential increases by an amount proportional to the weight of the synaptic connection through which the spike came. If the increased membrane potential does not exceed the threshold value, then it starts to decrease with the characteristic time τ_m (relaxation period), until a new

*E-mail: ilyin0048@gmail.com

spike entries this neuron. When the threshold potential is exceeded, the neuron emits a spike, after which the membrane potential drops to a minimum state (relaxation level). This state is retained for some time, called the refractory period of the neuron, t_{ref}.

In spiking neural networks there is another dynamic aspect, plasticity, which works at the level of two neurons (preneuron and postneuron) with synaptic connection between them. In this article, we use Spike-Timing-Dependent Plasticity (STDP) [4, 5]. There are two branches of the STDP dynamics. The first one (positive)—if a spike from a preneuron arrives at a postneuron before the postneuron emits a spike, then the weight of the corresponding synaptic connection increases. The second branch (negative)—if a postneuron emits a spike before a spike from a preneuron arrives at it, then the weight of the synaptic connection between them decreases.

Note that the STDP dynamic was discovered experimentally by neuroscientists [5, 6]. At the same time, it has a historical predecessor—Hebb's rule [7], in which there was no negative branch of weight change. The Hebb's rule was proposed to train neural networks at the synaptic level. Note, that both branches of the STDP dynamics play a critical role in our research.

All dynamic aspects of a spiking neural network are formulated at the local level of basic dynamic elements—neurons and synaptic connections. The STDP rule is also formulated locally—it involves a pair of neurons with synaptic connection between them. At the same time, learning a spiking neural network is understood as an optimization of the network in a whole. There is a problem of bridging the gap between the local and global levels in the dynamics of spiking neural networks—how to move from local neurodynamic phenomena to global processes that could be interpreted, for example, as the training of spiking neural networks. This problem is of fundamental character for the concept of machine learning, which remains unresolved at the moment. Note that in neuroscience, the same problem is far from being solved.

The STDP impact on the dynamics of weight distribution in the spiking network may be considerate as follows. The weights are increased of those incoming connections through which the pre-spikes arrive actively just before the neuron emits outgoing spike. In case of such active incoming environment the neuron became to be more active, and its outgoing activity will increase, enhancing activity of next neurons. This would mean that the STDP dynamics can generate paths of active neurons at the scale of the digraph. Following these assumptions, we formulatethe encoding hypothesis:

When the input signal is repeatedly fed into the spiking neural network, the STDP dynamics increases synaptic weights along the paths of active neurons, while reducing the weights of other synaptic connections. As a result, a directed subgraph (path complex) consisting of edges with large synaptic weights will be identified in the network for this signal. These path complexes will correspond uniquely for input signals.

The starting value for all synaptic weights of the spiking network is chosen to be 0.5. Then, if the encoding hypothesis holds, then an important phenomenon will be bimodal distribution of synaptic weights in the digraph after some feeds of the signal. This means that there should be no edges with weights in some range around the starting value of 0.5. The bimodal distribution open the possibility of numerical highlighting of the path complexes under discussion through the cut off of edges with small values of synaptic weights.

In research we will use the mathematics of path complexes in directed graphs [8, 9].

For the chosen digraph architecture, the set of parameters of the spiking neural network is selected so that for each input signal, its unique path complex manifests itself. The corresponding set of path complexes is analyzed by methods of algebraic topology. Simplexes of different dimensions are identified and homologies are computed for each of path complex. As we will see further this set of algebra-topological structures characterizes input signals uniquely.

The path complexes obtained for the input signals can be represented as points in Euclidean space, the unit vectors of which correspond to the edges of the digraph. If the minimum distance between these points is greater than zero, then this will means the encoding hypothesis formulated above is hold.

As a result, we can talk about a new method of encoding input signals in terms of path complexes in the digraph of a spiking neural network. On this basis, it will be available for the development of new types of data analysis tools without the (resource-intensive) step of training a neural network on large datasets.

In the following sections of the article we discuss:

- the spike neural network model, Section 2;
- model of the input signals, Section 3;
- computational experiments and bimodality in the distribution of weights, Section 4;
- mapping of path complexes into Euclidean space, Section 5;

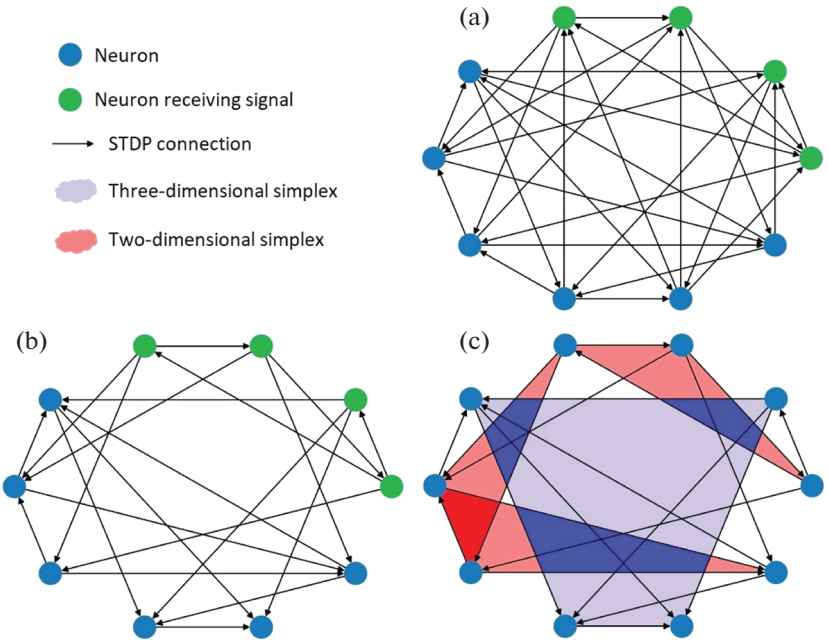

Fig. 1. (a) Topology of the SNN digraph, (b) an example of a path complex with 10 vertices and 16 edges, (c) visualization of two 2D simplexes (triangles, red) and one 3D simplex (tetrahedron, blue) on this path complex.

- algebra-topological portraits of path complexes, Section 6.

The Conclusions section discusses the results of the conducted research and computational experiments.

The literature presents the results of studies on synchronous excitation of groups of neurons in spiking neural networks [10]. One of these results is the observation of polychronic groups of neurons [11], between which (excitatory) synaptic connections are abnormally strengthened as a result of neural activity. In such groups, stimulation of a subset of neurons activates excitation of the entire group as a whole. As a result, polychromic groups of neurons can be considered as separate operational units of spiking neural networks. These results may be assessed as a step towards solving the fundamental problem formulated above of the transition from local neuronal dynamic phenomena to global processes in the network, which could be interpreted as cognitive processes.

In the context of our research, we also note the publications [12, 13], which present the results of studies of the problem of unified cognitive mechanism of memory at two significantly differed time scales of dynamic processes in the brain: at the scale of spiking neurons (tens of milliseconds) and the scale of astrocytic modulation of synaptic transmissions (minutes). These studies aim to address the problem of the gap in time scales between neurodynamic processes and cognitive processes in the brain.

An important applied feature of spiking neural networks is the possibility of hardware implementation on specialized neuromorphic chips, for example, of the memristive type [14, 15]. This can potentially reduce energy consumption compared to artificial neural networks running on traditional computing devices, such as graphics processors. This feature also actualizes research in the field of spiking networks.

2. SNN MODEL

The architecture of the selected spiking neural network model (thereafter SNN) includes 10 neurons and 30 synaptic connections. Three directed edges enter and three edges exit each vertex of the digraph in this model. The SNN model is chosen in such a way that the digraph structures are sufficient for the manifestation of path complexes separating a set of input signals. Due to the limitation of the number of input and output edges for each vertex, the manifested path complexes can contain 0-dimensional (vertices), 1-dimensional (edges), 2-dimensional (triangles), and 3-dimensional (tetrahedra) simplexes. Such simplexes allow for visualization, which was the motivation for limiting the number of incoming and outgoing edges at the vertices of the digraph.

In Fig. 1a an SNN digraph with 10 vertices and 30 edges is presented. Four vertices (green marks) are shown as vertices, receiving input spikes from signal sources. At the bottom left (Fig. 1b) an example of a path complex is shown. And at the bottom

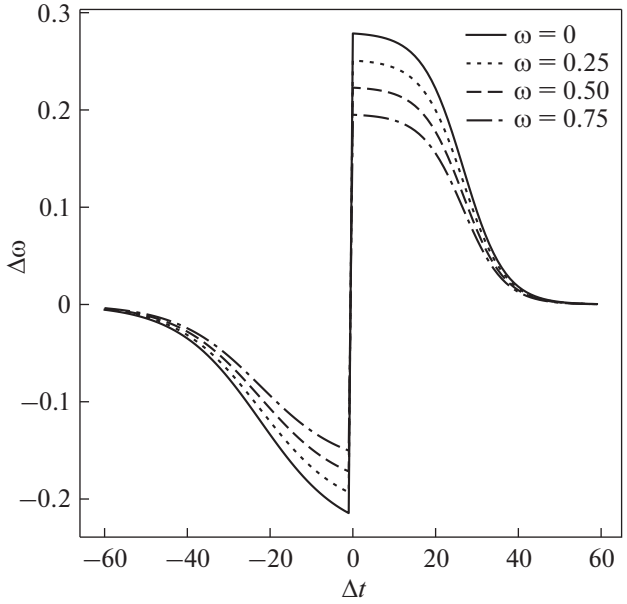

Fig. 2. STDP based on the approximation of the conductivity of nanocomposite memristor.

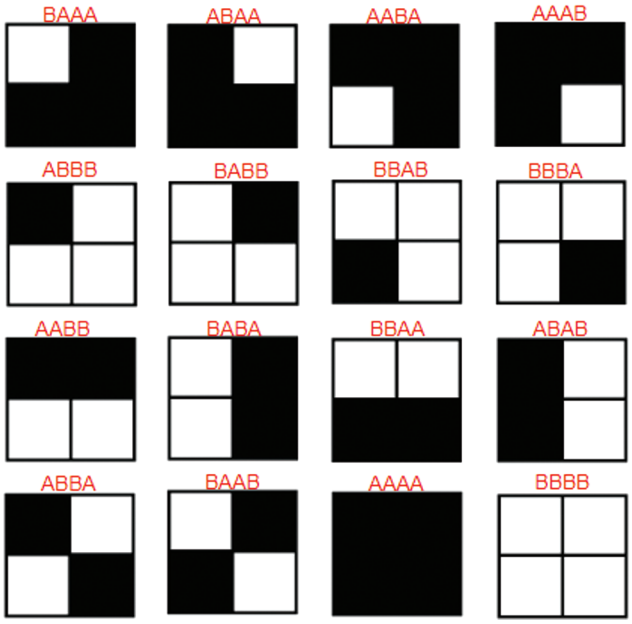

Fig. 3. Input signals: each signal is represented as 2×2 square of pixels, where A is a black pixel, B is a white pixel.

right (Fig. 1c) examples of two 2D simplexes (triangles, red) and one 3D simplex (tetrahedron, blue) are visualized on this path complex.

The SNN model includes a specific implementation of the STDP dynamics. There are many such implementations in the literature. In our studies, we have chosen the variant of STDP (see Eq. (1)) that can be implemented on nanocomposite memristive chips [16]. In such an implementation, the following equations [17] are used for the two branches of the STDP dynamics (positive and negative, see Fig. 2):

$$\Delta\omega(\Delta t) = \begin{cases} A^+\omega\left[1+\tan\left(\frac{\mu_+-\Delta t}{\tau_+}\right)\right], & \Delta t > 0; \\ A^-\omega\left[1+\tan\left(\frac{\Delta t-\mu_-}{\tau_-}\right)\right], & \Delta t < 0. \end{cases} \quad (1)$$

Here, $\Delta t = t_{\text{post}} - t_{\text{pre}}$; A^+ (>0) and A^- (<0) are the coefficients of potentiation and depression; τ_+, τ_-, μ_+, and μ_- are the time constants of the STDP dynamics; $\Delta\omega$ is the change in the ω, the current value of the synaptic weight.

3. MODEL OF THE INPUT SIGNALS

The model of input signals includes 16 signals, each consists of 4 binary pixels. Figure 3 shows images of input signals, in which each of the four pixels can be in one of two states: A—black, B—white.

The vertices of the SNN digraph are numbered from 0 to 9. Four vertices are designated as input vertices (their numbers are 0, 1, 2, and 3). During the first 20 ms (the signal feed window), the signal is fed. The pixels in these images are numbered in the same order for all signals, say as 0, 1, 2 and 3. The fed rule is the following—for all signals four pixels are fed on four input vertices uniformly over the signals: 1st pixel is fed on the 1st input neuron, ..., 4th pixel is fed on the 4th input neuron, as shown in Fig. 4. During the next 80 ms there is no input signals. We will denote this 100 ms interval as an epoch.

If a pixel is in state A (black), it is encoded by four spikes, which are fed at times of 2, 7, 12, and 17 ms within the signal feed window. If a pixel is in state B (white), it is encoded by one spike, which is fed to its input neuron at time 10 ms in the signal feed window.

4. COMPUTATIONAL EXPERIMENTS. BIMODALITY

For the computational experiments, the SNN model and input data model described in Sections 2 and 3 were used with the following set of parameters:

- general parameters: spike duration 0.1 ms, synaptic delay $t_{\text{syn}} = 0.1$ ms;
- neuron parameters: refractory period $t_{\text{ref}} = 1$ ms, membrane potential relaxation period $\tau_m = 3$ ms, threshold voltage $V_{\text{th}} = 16$ mV, resting voltage $V_{\text{rest}} = -65$ mV;
- STDP parameters: $A^+ = 0.14$, $A^- = -0.12$, $\tau_+ = 10$ ms, $\tau_- = 20$ ms, $\mu_+ = 26.7$ ms, $\mu_- = 22.3$ ms.

Each of the 16 input signals is fed into the SNN multiple times (200 epochs). Before the first epoch, all synaptic weights are set to the starting state equal to 0.5. During the computational experiment, the weights are changed by the STDP dynamics. For each signal, the resulting distributions of the SNN digraph weights are recorded for further analysis after each of 200 epochs.

To check whether a bimodal weight distribution has been established, intervals of weights around the starting value 0.5, in which there are no edges, were computed for each signal i and epoch j_{ep}:

$$\omega^i_{\min}(j_{\text{ep}}) < 0.5 < \omega^i_{\max}(j_{\text{ep}}), \tag{2}$$

where $\omega^i_{\min}(j_{\text{ep}})$ and $\omega^i_{\max}(j_{\text{ep}})$ are lower and upper boundaries of these intervals (thereafter, bimodal intervals).

For the full set of signals from the lower boundaries of the bimodal intervals (see Eq. (2)) the maximum value is selected for each epoch, $\omega_{\min}(j_{\text{ep}})$, and from the upper boundaries the minimum value is selected, $\omega_{\max}(j_{\text{ep}})$. We obtain bimodal intervals at different epochs for the entire set of signals according to Eq. (3)

$$\omega_{\min}(j_{\text{ep}}) < 0.5 < \omega_{\max}(j_{\text{ep}}). \tag{3}$$

It follows from Fig. 5 that bimodal weight distribution is stabilized after 50th epoch, with sizes of the bimodal intervals more than 0.6. It is worth to note that upper boundary of this interval, $w_{\max}$, is stabilized starting already from 25th epoch at the level of 0.7. This makes it possible to identify path complexes with large weights using a cutoff less then 0.7.

5. MAPPING PATH COMPLEXES INTO EUCLIDEAN SPACE

In this and next sections for all signals we will use the weight distribution after 200th epoch.

There is an obvious way to introduce the Euclidean metric on the set of path complexes. For this purpose, each edge of the digraph corresponds to an unit vector of the Euclidean space $\mathcal{E}$, which, in our case, will be 30-dimensional. The mapping of the path complex π into $\mathcal{E}$ can be defined in two ways:

$$\pi \to \sum_{k=1}^{30} \alpha^\pi_k e_k \in \mathcal{E}, \tag{4}$$

$$\pi \to \sum_{k=1}^{30} \alpha^\pi_k \omega_k e_k \in \mathcal{E}, \tag{5}$$

where $\alpha^\pi_k = 1$ if $k \in \pi$, and $\alpha^\pi_k = 0$ otherwise. Here ω_k are the synaptic weights of digraph edges. Note

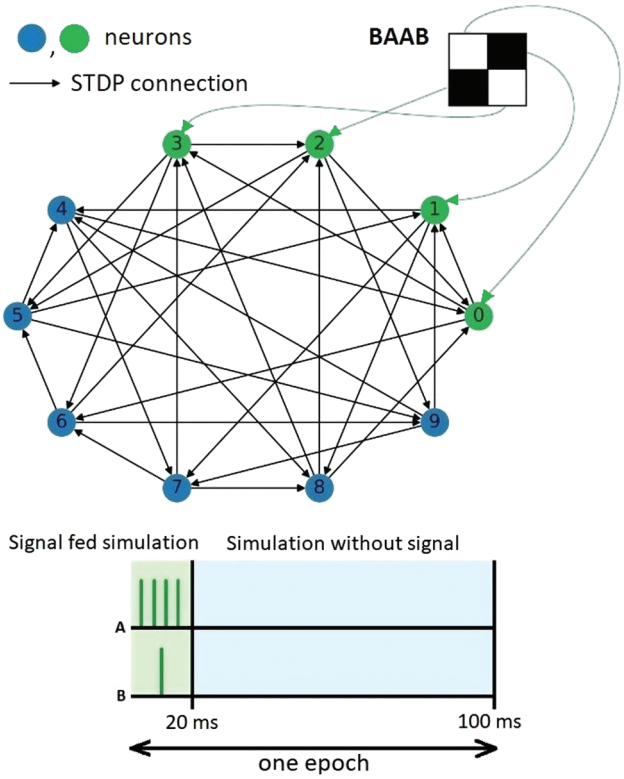

Fig. 4. The scheme of the BAAB signal feed to the input neurons. On the top the indication from which pixel in the signal to which input neuron the spikes come. On the bottom one epoch of the signal feed is shown.

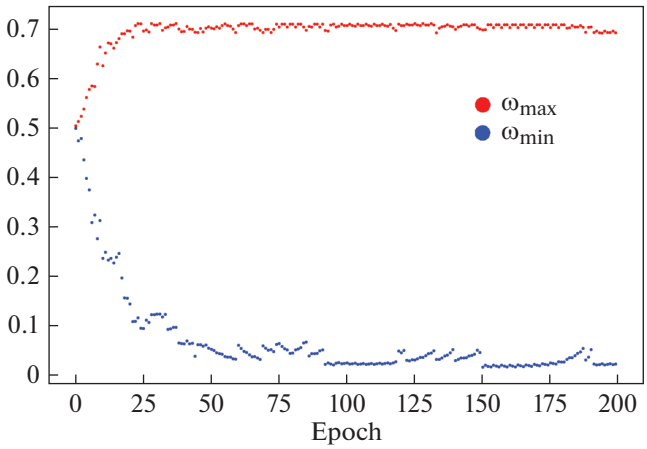

Fig. 5. Upper $w_{\max}$ and lower $w_{\min}$ boundaries for the bimodal interval (3) in dependence on epoch.

that in the formulas (4), (5), only the weights of edges on the path complex π contribute, since the contributions of other edges are nullified by the coefficient α^π_k.

The mappings (4), (5) match two points in $\mathcal{E}$ to the same path complex. Thus, we obtain two metrics in the space of path complexes.

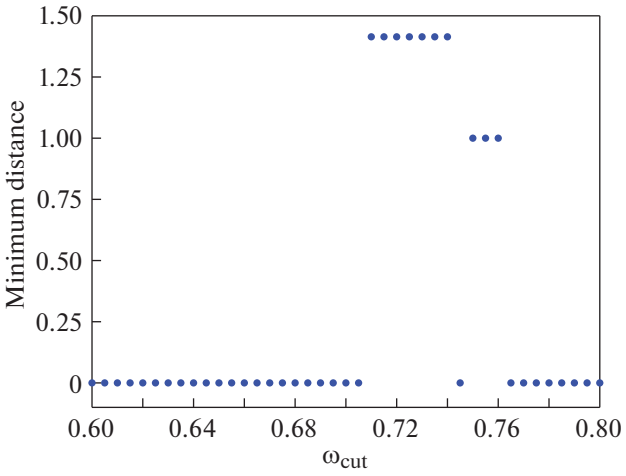

Fig. 6. Minimum distance along the first metric (excluding weights) between pairs of path complexes in dependence on the cutoff value, ω_{cut}.

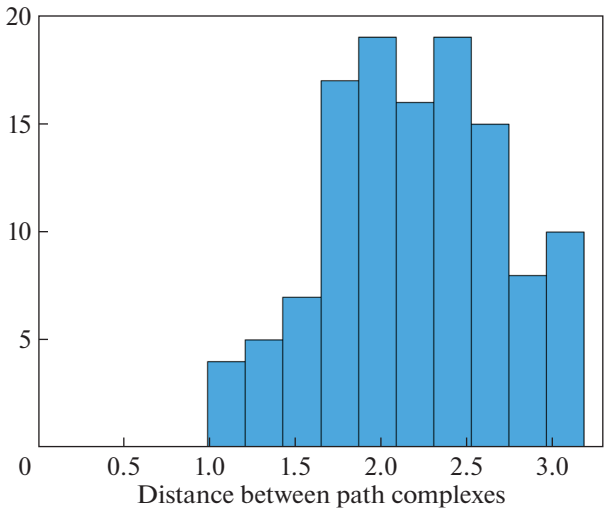

Fig. 7. Histogram of distances from Table 1 between path complexes (input signals).

In the case of (4), distances are computed without taking into account the weights on the edges of the path complex. Such metric will be used to compare path complexes as digraphs. Obviously, if such distance between two path complexes is zero, then they coincide as digraphs.

In the case of (5), the distances are computed taking into account the weights on the edges of the path complex. Such distances will allow us to estimate the proximity of path complexes taking into account information from the dynamic action of STDP. This may be important, for example, for estimating the proximity of path complexes at different degrees of signal noisiness. If the noisiness is small enough, it may turn out that the path complexes, as digraphs, are coincided. And it will be possible to distinguish them only by weight distributions, i.e., with the help of the second metric (5).

Let us first analyze distances between pairs of path complexes, computed by the first metric (4). The plot in Fig. 6 shows dependence of the minimum distance between pairs of path complexes (input signals) computed for different values of ω_{cut}. If $\omega_{\text{cut}} < 0.7$, some pairs of path complexes appear with zero distance between them, which means that they completely coincide as digraphs. In the interval $0.71 < \omega_{\text{cut}} < 0.74$, the minimum distance is 1.4. At larger cutoffs, the path complexes become disconnected digraphs, and then zero distances appear again. We can conclude that encoding of input signals in terms of path complexes is optimal for $0.71 < \omega_{\text{cut}} < 0.74$.

Later in this section and in the next section, we will use $\omega_{\text{cut}} = 0.71$ to cut off edges with small weights in order to identify path complexes as encoding input signals.

Now, let us look at the distances between the path complexes (input signals) computed by the second metric (with weights). These distances are presented in Table 1. The minimum distances in this table is equal to 1.1.

6. ALGEBRA-TOPOLOGICAL PORTRAIT OF A PATH COMPLEX

We define the algebra-topological portrait (*ATportrait*) of the input signal as the set of simplexes and homologies in the corresponding path complex.

To find homologies, we use the theory of homologies of path complexes presented in [8]. The notion of path complex unifies and generalizes the notions of simplicial complex and digraph. A complex of paths P on a finite set V is a set of paths (sequences of points) on V such that if a path v belongs to P, then the truncated path obtained from v by removing the first or the last point belongs to P also. For a given path complex P, all paths in P are called allowed. Obviously, any directed graph defines a path complex in which the allowed paths go along the directed edges of the digraph.

To define the homology of a path complex P with a set of vertices V, one introduces the space of allowed n-paths (paths out of n vertices)

$$A_n = \left\{ \sum_{i_0,\ldots,i_n \in V} v^{i_0\ldots i_n} e_{i_0\ldots i_n} : i_0 \ldots i_n \in P \right\}, \quad (6)$$

where $v^{i_0\ldots i_n}$ are real coefficients and $e_{i_0\ldots i_n}$ is an elementary n-path (an arbitrary sequence of $p+1$ vertices from V). On this space we introduce the boundary operator

$$\partial : A_n \to A_{n-1},$$

Table 1. Distances between path complexes computed using the second metric (5), after 200th epoch and $\omega_{\text{cut}} = 0.71$. The numeration in the first column and the first row corresponds to the signals as follows: 1—BAAA, 2—ABAA, 3—AABA, 4—AAAB, 5—ABBB, 6—BABB, 7—BBAB, 8—BBBA, 9—AABB, 10—BABA, 11—BBAA, 12—ABAB, 13—ABBA, 14—BAAB, 15—AAAA, 16—BBBB

	1	2	3	4	5	6	7	8	9	10	11	12	13	14	15	16
1	0	–	-	–	–	–	–	–	–	–	–	–	–	–	–	–
2	2.3	0	-	–	–	–	–	–	–	–	–	–	–	–	–	–
3	2.8	2.3	0	–	–	–	–	–	–	–	–	–	–	–	–	–
4	2.4	2.4	2.5	0	–	–	–	–	–	–	–	–	–	–	–	–
5	2.7	1.7	1.6	2.7	0	–	–	–	–	–	–	–	–	–	–	–
6	1.9	1.1	2.5	2.3	2.0	0	–	–	–	–	–	–	–	–	–	–
7	2.3	2.1	3.1	2.4	2.7	1.8	0	–	–	–	–	–	–	–	–	–
8	2.7	1.9	2.2	2.5	1.6	1.9	2.5	0	–	–	–	–	–	–	–	–
9	2.9	2.4	1.4	2.4	1.8	2.6	3.0	2.0	0	–	–	–	–	–	–	–
10	2.5	2.3	1.1	2.2	1.9	2.5	3.2	2.1	1.8	0	–	–	–	–	–	–
11	1.7	1.7	2.9	2.8	2.6	1.4	2.0	2.3	3.0	2.9	0	–	–	–	–	–
12	2.4	1.6	2.5	2.2	2.0	2.0	1.8	1.9	2.5	2.5	1.9	0	–	–	–	–
13	2.5	1.8	2.0	2.6	1.4	1.8	2.5	1.4	2.2	2.2	2.1	1.9	0	–	–	–
14	3.0	2.9	3.2	2.6	3.2	3.0	2.6	3.0	2.9	3.2	2.9	2.6	3.2	0	–	–
15	2.1	1.8	2.0	2.2	1.8	2.0	2.6	1.7	2.2	1.7	2.2	1.7	1.9	2.7	0	–
16	1.9	1.2	2.2	2.0	1.7	1.1	1.9	1.5	2.3	2.2	1.8	1.6	1.4	2.8	1.7	0

which is defined on the elementary paths by

$$\partial e_{i_0 \dots i_n} = \sum_{k=0}^{n} (-1)^k e_{i_0 \dots \widehat{i}_k \dots i_n},$$

where $\widehat{i}_k$ means the omission of the index i_k.

By definition, for any $n \geq 0$, vector space of n-dimensional homologies is a factor space

$$H_n = \text{Ker}\partial|_{\Omega_n} / \text{Im}\partial|_{\Omega_{n+1}},$$

where $\partial|_{\Omega_n}$ is the contraction of the boundary operator to the space of ∂-invariant n-paths

$$\Omega_n = \{v \in A_n : \partial v \in A_{n-1}\}.$$

Above we used the term *simplex* without giving strict mathematical definition for it, limiting ourselves to geometric notations. Following the [8, 9], we define a digraph-simplex of dimension d as a directed graph with $d+1$ vertices, each pair of vertices connected by a directed edge, and which has trivial vector spaces of n-dimensional homologies for $n \geq 1$. The latter condition is ensured by the fact that the vector spaces of n-dimensional homologies of the simplex are trivial for $n \geq 1$. A digraph-simplex defined in this way is topologically equivalent to a simplex.

The count of simplexes for the *ATportrait* of a path complex is performed with the following conditions: the number of 2-dimensional simplexes does not include faces of the tetrahedrons (3-dimensional simpelexes), the number of 1-dimensional simplexes does not include edges of 2-dimensional and 3-dimensional simplexes. We will denote these features as: N_1^s, N_2^s, and N_3^s correspondingly. Moreover, the path complexes obtained for the input signals can have only 1-dimensional homologies—closed directed cycles composed of edges. This is a consequence of limitation on numbers of vertices and synaptic connections in the SNN digraph. There can be several such cycles, up to three. For each cycle we will specify the number of its edges, n_c^h.

Thus, we will represent *ATportrait* for each input signal as a vector with 7 components:

$$ATportrait = \left(N_1^s, N_2^s, N_3^s, N^h, n_1^h, n_2^h, n_3^h\right).$$

The results of computing these characteristics for all input signals are presented in Table 2. Analysis of this table allows us to conclude that each signal has its own unique *ATportrait*.

Table 2. *ATportraits* for path complexes obtained for the input signals (after 200th epoch, and $\omega_{\text{cut}} = 0.71$)

Signal	N_1^s	N_2^s	N_3^s	N^h	n_1^h	n_2^h	n_3^h
BAAA	6	2	1	2	14	8	–
ABAA	3	9	0	1	21	–	–
AABA	5	2	2	2	16	18	–
AAAB	2	4	1	2	14	8	–
ABBB	3	3	2	2	17	18	–
BABB	2	5	3	1	23	–	–
BBAB	6	1	2	1	15	–	–
BBBA	3	8	0	2	18	18	–
AABB	2	6	2	2	19	20	–
BABA	4	6	0	2	15	13	–
BBAA	5	4	1	1	20	–	–
ABAB	9	3	0	3	9	15	15
ABBA	1	5	2	1	20	–	–
BAAB	8	2	0	2	8	9	–
AAAA	6	5	0	2	13	13	–
BBBB	2	7	1	2	20	20	–

7. CONCLUSIONS

In Sections 5 and 6 two methods were proposed for comparing path complexes that are encodings of input signals: computation of Euclidean distances between path complexes and algebraic-topological portraiturings.

Each of these methods confirms the validity of the encoding hypothesis of input signals in terms of path complexes formulated in the Introduction.

This result was obtained for simple models, SNN (Section 2) and input data (Section 3). The limitations of the chosen SNN model architecture (10 neurons with 3 incoming and 3 outgoing synaptic connections) allowed visualization of path complexes. In addition, the dimensions of simplexes are limited to 3, and only 1-dimensional homology is possible.

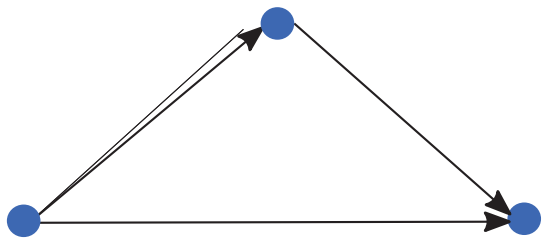

Fig. 8. Digraph-simplex of dimension 2 (triangle).

Such structures can be visualized, which increases the interpretability of the results. These architectural limitations also simplified the research and computational experiments. At the same time, we note that the encoding hypothesis nevertheless received significant support, justifying further research.

The following comments can be made on the two methods of comparing path complexes (input signal encodings) proposed in Sections 5 and 6. The Euclidean metric method for comparing path complexes is based on the (obvious) fact that a path complex is uniquely determined by a set of edges in a directed graph. On this basis, in Section 5 we proposed definitions of two metrics (4 and 5) for numerically comparing path complexes (input signals). We note that the representation of path complexes in the edges terms used in the definitions of these metrics can be interpreted as a conjuction to the representation in terms of admissible paths over vertices in the SNN digraph (see Eq. (6)). One can suppose that comparison of path complexes based on Euclidean metrics (Eqs. (4) and (5)) and by the *ATportraituring* could be not effective for a deeper structural analysis of input signals. In this connection, mathematics of cohomologies, which are mathematically conjugate objects in relation to homologies, may be interesting for such an analysis.

The next comment concerns the proposed input signal encoding method as a whole. This method is, in fact, a new tool for analyzing input signals. Our research showed that this tool requires fine tuning of the SNN model parameters and the parameter for cutting off edges with small weights, ω_{cut}. For example, for the relaxation period of a neuron in the SNN model, we used the value $\tau_m = 3$ ms in the computational experiments. If this parameter is less, $\tau_m < 2$ ms, or greater, $\tau_m > 5$ ms, the problems with bimodality will appear. Further, in Section 5 it was found that the proposed method turned out to be sensitive to the parameter ω_{cut} for cutting off edges with small weights.With the parameters used in the computational experiments, a rather narrow interval for this cutoff parameter turned out to be acceptable, $0.71 < \omega_{\text{cut}} < 0.74$. Similar problems are observed for the method of separating input signals by algebraic-topological portraits of path complexes. We expect that for complicated models of the spiking neural network and input signals, a more complete analysis of the window of acceptable parameter values will be required to get complete separation input signals by their encodings in terms of path complexes.

Finally, we note that encoding input signals in internal terms of the spiking neural network can be considered as an initial step in developing, for example, methods for classifying datasets. Classical machine learning methods (not spiking ones) require

a large datasets for training. Our further research will be aimed at studying the proposed method in the direction of reducing the dependence on such a resource-intensive stage as labeling training data when solving classification problems.

ACKNOWLEDGMENTS

This work has been carried out using computing resources of the Federal collective usage center Complex for Simulation and Data Processing for Mega-science Facilities at the National Research Centre "Kurchatov Institute," http://ckp.nrcki.ru/.

FUNDING

This work was supported by the Russian Science Foundation, project 23-11-00260, https://rscf.ru/project/23-11-00260/.

CONFLICT OF INTEREST

The authors of this work declare that they have no conflicts of interest.

REFERENCES

1. F. Ponulak and A. Kasinski, Acta Neurobiol. Exp. **71**, 409 (2011). https://doi.org/10.55782/ane-2011-1862
2. J. Bang-Jensen and G. Z. Gutin, *Digraphs: Theory, Algorithms and Applications*, Springer Monographs in Mathematics (Springer, London, 2008). https://doi.org/10.1007/978-1-84800-998-1
3. C. Teeter, R. Iyer, V. Menon, N. Gouwens, D. Feng, J. Berg, A. Szafer, N. Cain, H. Zeng, M. Hawrylycz, Ch. Koch, and S. Mihalas, Nat. Commun. **9**, 709 (2018). https://doi.org/10.1038/s41467-017-02717-4
4. W. Gerstner, R. Kempter, J. L. van Hemmen, and H. Wagner, Nature **383**, 76 (1996). https://doi.org/10.1038/383076a0
5. H. Markram, J. Lübke, M. Frotscher, and B. Sakmann, Science **275**, 213 (1997). https://doi.org/10.1126/science.275.5297.213
6. G.-Q. Bi and M.-M. Poo, J. Neurosci. **18**, 10464 (1998). https://doi.org/10.1523/jneurosci.18-24-10464.1998
7. D. O. Hebb, J. Clin. Psychol. **6**, 335 (1949).
8. A. Grigor'yan, Y. Lin, Yu. Muranov, and S.-T. Yau, arXiv Preprint (2012). https://doi.org/10.48550/arXiv.1207.2834
9. A. A. Grigor'yan, Yo. Lin, Yu. V. Muranov, and S.-T. Yau, J. Math. Sci. **248**, 564 (2020). https://doi.org/10.1007/s10958-020-04897-9
10. E. M. Izhikevich, J. A. Gally, and G. M. Edelman, Cereb. Cortex **14**, 933 (2004). https://doi.org/10.1093/cercor/bhh053
11. F. C. Hoppensteadt and E. M. Izhikevich, *Weakly Connected Neural Networks*, Applied Mathematical Sciences, Vol. 126 (Springer, New York, 1997). https://doi.org/10.1007/978-1-4612-1828-9
12. S. Yu. Gordleeva, Yu. A. Tsybina, M. I. Krivonosov, M. V. Ivanchenko, A. A. Zaikin, V. B. Kazantsev, and A. N. Gorban, Front. Cell. Neurosci. **15**, 631485 (2021). https://doi.org/10.3389/fncel.2021.631485
13. S. Gordleeva, Yu. A. Tsybina, M. I. Krivonosov, I. Y. Tyukin, V. B. Kazantsev, A. Zaikin, and A. N. Gorban, IEEE Trans. Neural Networks Learn. Syst. (2023). https://doi.org/10.1109/tnnls.2023.3335450
14. A. Minnekhanov, A. Matsukatova, A. Trofimov, A. Nesmelov, S. Zavyalov, V. Demin, and A. Emelyanov, ACS Appl. Mater. Interfaces **15**, 54996 (2023). https://doi.org/10.1021/acsami.3c13956
15. J. Kim, S. Lee, Ye. Seo, and S. Kim, J. Chem. Phys. **160**, 144703 (2024). https://doi.org/10.1063/5.0202610
16. V. A. Demin, D. V. Nekhaev, I. A. Surazhevsky, K. E. Nikiruy, A. V. Emelyanov, S. N. Nikolaev, V. V. Rylkov, and M. V. Kovalchuk, Neural Networks **134**, 64 (2021). https://doi.org/10.1016/j.neunet.2020.11.005
17. A. Sboev, D. Vlasov, R. Rybka, Yu. Davydov, A. Serenko, and V. Demin, Mathematics **9**, 3237 (2021). https://doi.org/10.3390/math9243237